OPEN ACCESS

University of BRISTOL

Lohans, C. T., Wang, D. Y., Jorgensan, C., Cahill, S. T., Clifton, I. J., McDonough, M. A., Oswin, H., Spencer, J., Domene, C., Claridge, T. D. W., Brem, J., & Schofield, C. J. (2017). 13C-Carbamylation as a mechanistic probe for the inhibition of class D β-lactamases by avibactam and halide ions. *Organic and Biomolecular Chemistry*, *15*(28), 6024-6032. https://doi.org/10.1039/C7OB01514C

Publisher's PDF, also known as Version of record

License (if available):
CC BY

Link to published version (if available):
10.1039/C7OB01514C

Link to publication record in Explore Bristol Research
PDF-document

This is the final published version of the article (version of record). It first appeared online via RSC at https://pubs.rsc.org/en/Content/ArticleLanding/2017/OB/C7OB01514C#!divAbstract . Please refer to any applicable terms of use of the publisher.

University of Bristol - Explore Bristol Research
General rights

This document is made available in accordance with publisher policies. Please cite only the published version using the reference above. Full terms of use are available:
http://www.bristol.ac.uk/red/research-policy/pure/user-guides/ebr-terms/

Electronic Supplementary Material (ESI) for Organic & Biomolecular Chemistry.
This journal is © The Royal Society of Chemistry 2017

Supporting Information

^{13}C-Carbamylation as a Mechanistic Probe for the Inhibition of Class D β-Lactamases by Avibactam and Halide Ions

Christopher T. Lohans[1], David Y. Wang[1], Christian Jorgensen[2], Samuel T. Cahill[1], Ian J. Clifton[1], Michael A. McDonough[1], Henry P. Oswin[3], James Spencer[3], Carmen Domene[1,2], Timothy D.W. Claridge[1], Jürgen Brem[1*], and Christopher J. Schofield[1*]

[1]Department of Chemistry, University of Oxford, Oxford, UK, OX1 3TA;

[2]Department of Chemistry, King's College London, London, UK, SE1 1DB;

[3]School of Cellular and Molecular Medicine, University of Bristol, Bristol, UK, BS8 1TD.

*Address correspondence to:

Prof. Christopher Schofield, christopher.schofield@chem.ox.ac.uk, Tel: +44 (0)1865 275625, Fax: +44 (0)1865 285002

Dr. Jürgen Brem, jurgen.brem@chem.ox.ac.uk

Supporting Information Contents

Supplemental Methods

Modelling Methods

The crystal structures of the dimeric OXA-10:avibactam complex with bromide, iodide, sodium, and carbon dioxide bound in the active site were used for QM/MM geometry optimization using the CP2K code[1] (http://cp2k.berlios.de). Each protomer was solvated using the Solvate plugin from VMD using a box of dimensions (80 × 80 × 80) $Å^3$. The systems were neutralized using a background NaCl solution with the Ionize plugin from VMD.[2] Details of the systems studied are summarized in Table S3.

For QM/MM geometry optimizations, the interaction energy for the QM region was computed via the QuickStep module within CP2K,[3, 4] with the FIST MM driver, and using a real-space multigrid technique for the electrostatic coupling between the QM and MM regions.[5, 6] The QM region was treated using density functional theory (DFT) with the BLYP exchange correlation energy functional[7, 8] employing the GTH pseudopotential of Goedecker *et al.*,[9, 10] and double-zeta valence plus polarization (DZVP) basis sets (optimized for BLYP) as implemented in CP2K. Br^-, I^- and Na^+ ions were described using the DZVP basis sets optimized for BLYP. The plane wave was expanded up to a density cut-off of 300 Ry. For the MM region, the CHARMM 27 force-field[11] was used with the TIP3P water model, using the FIST module within CP2K to calculate the MM interaction energy. Interactions between the QM and MM regions were calculated using the procedure of Laino *et al*.[6] MM and QM optimizations were performed separately, with the QM/MM interface described with the IMOMM link-atom method,[12] where positions of hydrogen capping atoms were expressed as a function of the coordinates of atoms forming the original bond, and the forces on the link atoms were accordingly redistributed. A scaling factor of 1.38 was applied to relate the MM carbon–carbon distances to the QM carbon–

hydrogen ones. Only the immediate active site was included in the QM region (Table S3); the rest of the protein was treated at the MM level. The QM/MM boundary was placed between the α- and β-carbons of Ser-67, Lys-70, Ser-115, and Trp-154. The total charge of the QM region in each system is summarized in Table S4. Geometry optimizations were performed for 5,000 iterations. For every step, the electronic structure was explicitly quenched to a tolerance of 10^{-14} hartree, and a convergence criteria of 10^{-3} for the RMS force and gradient was employed. The optimized geometries are given in Figure S14.

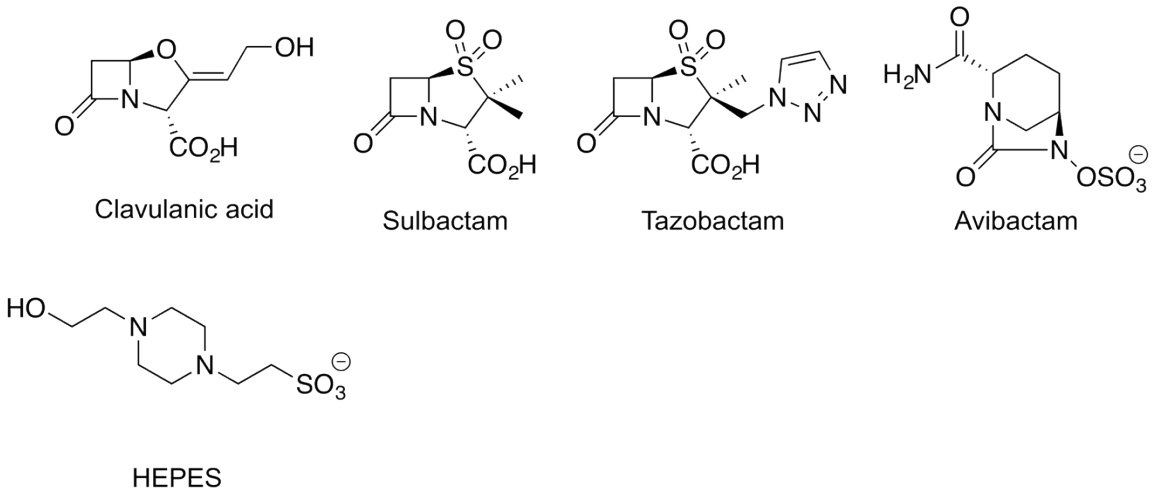

Figure S1. Structures of β-lactamase inhibitors used in our work and HEPES buffer. Chemical structures of clavulanic acid, sulbactam, tazobactam, avibactam, and 4-(2-hydroxyethyl)-1-piperazineethanesulfonic acid (HEPES).

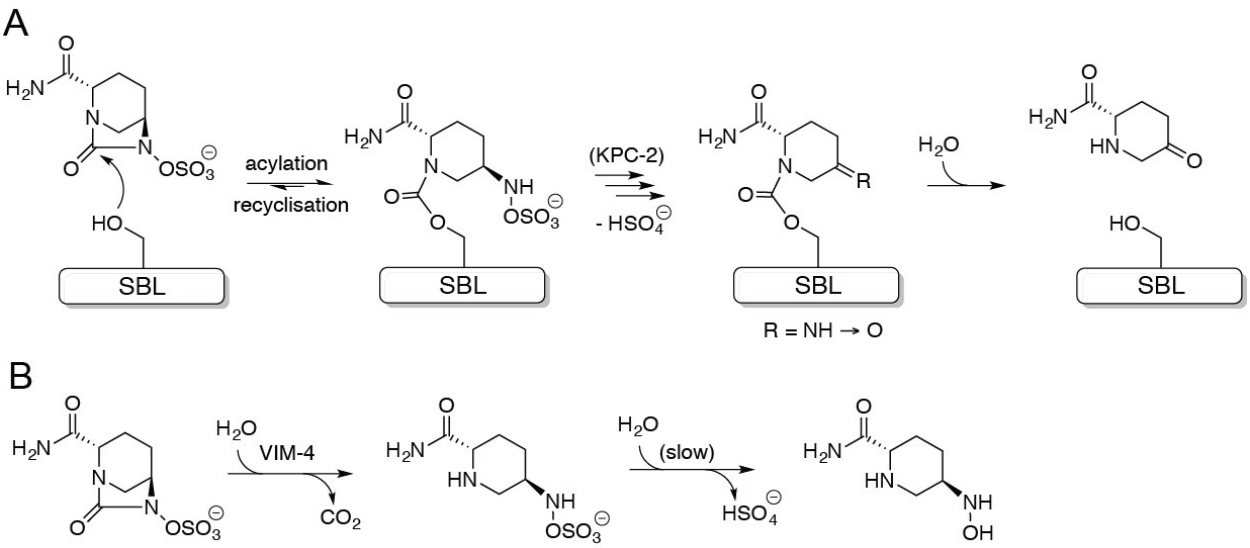

Figure S2. Hydrolysis of avibactam by serine and metallo-β-lactamases. (A) Outline mechanism for serine β-lactamase (SBL) acylation and recyclisation by avibactam, and observed mode of avibactam hydrolysis as observed with the *Klebsiella pneumoniae* carbapenemase-2 (KPC-2) SBL.[13] (B) Hydrolysis of avibactam as observed with the metallo-β-lactamase (MBL) Verona integron-encoded MBL-4 (VIM-4).[14]

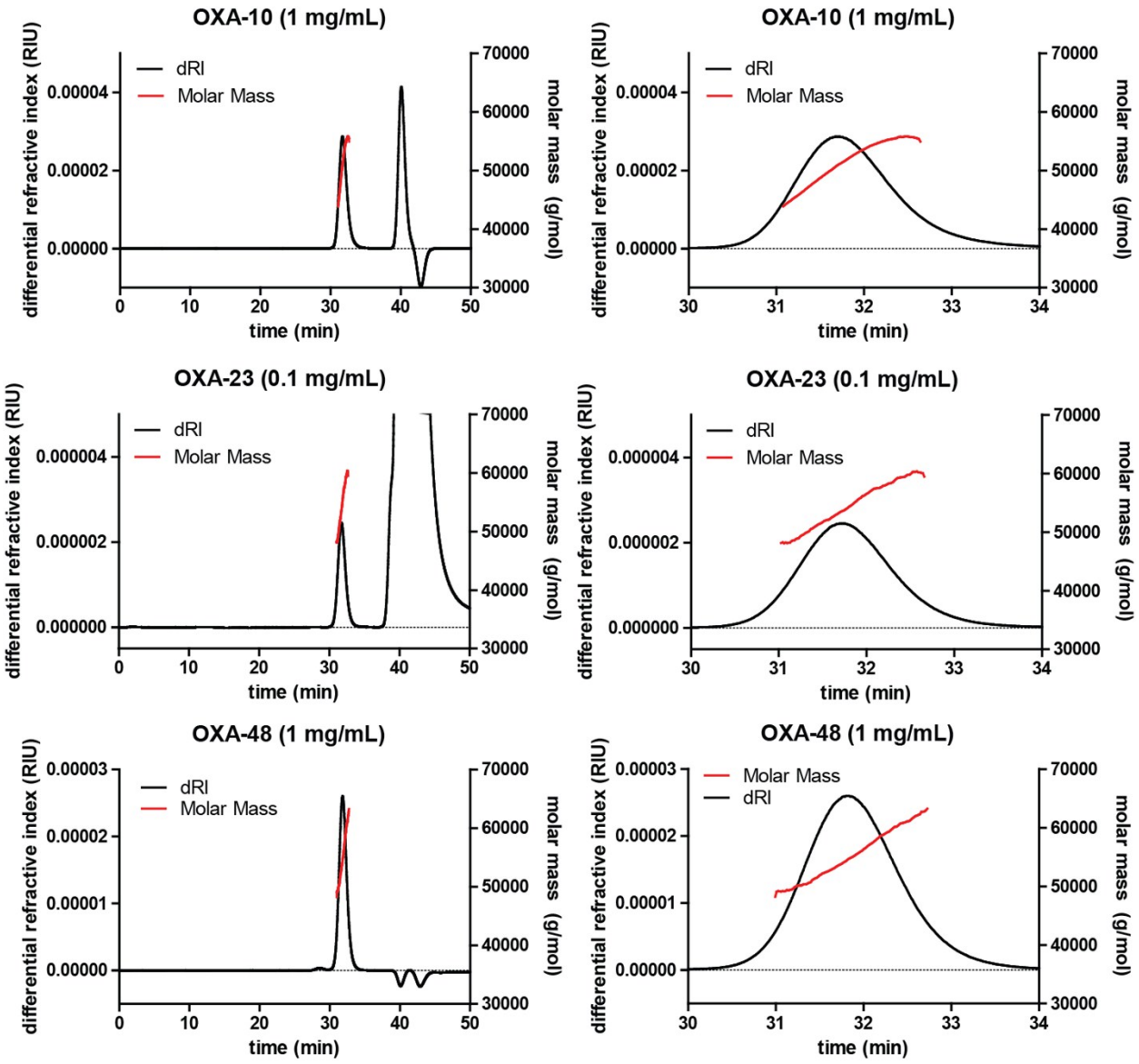

Figure S3. SEC-MALS characterisation of purified proteins. Size exclusion chromatography – multi-angle laser scattering (SEC-MALS) analyses showed the purity of purified OXA-10, OXA-23, and OXA-48, and the lack of aggregation. These data also suggested that all three enzymes were in a dimeric state (OXA-10: calculated 29.5 kDa, observed 51.2 kDa; OXA-23: calculated 31.0 kDa, observed 54.2 kDa; OXA-48: calculated 30.4 kDa, observed 55.2 kDa). Analyses were performed by Dr. David Staunton at the University of Oxford, Department of Biochemistry, Biophysics Facility. Chromatography was performed using a Superdex 75

HR10/30 column on a Shimadzu HPLC system, with a mobile phase of 50 mM sodium phosphate, pH 7.5. Detection used a Wyatt Dawn HELEOS-II 8-angle light scattering detector, a Wyatt Optilab rEX refractive index monitor, and an SPD20A UV/Vis detector.

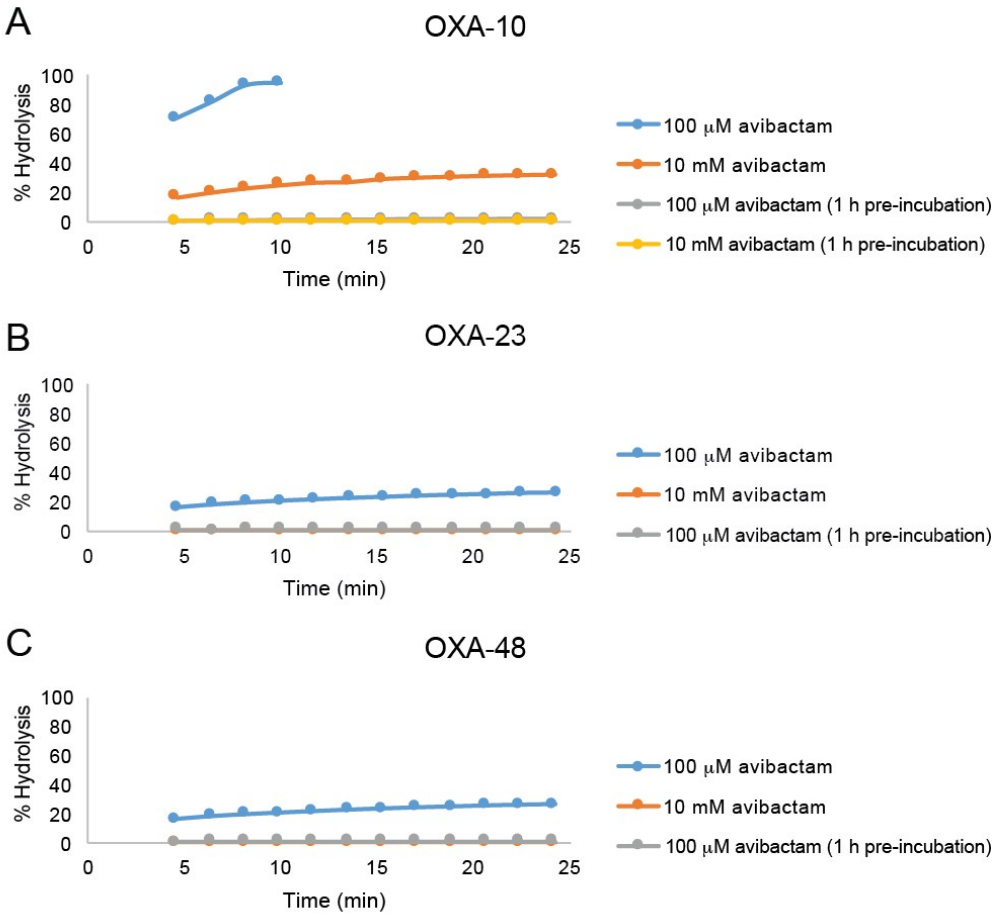

Figure S4. Pre-incubation of OXA enzymes with avibactam. The impact of avibactam on the hydrolysis rate of ampicillin by (A) OXA-10, (B) OXA-23, and (C) OXA-48 as observed by ^{1}H-NMR (700 MHz). Assays were either run immediately, or with a one hour pre-incubation step of avibactam and the OXA variant. The reactions consisted of 75 nM enzyme, either 100 μM or 10 mM avibactam, and 4 mM ampicillin in 50 mM Tris-d_{11}, pH 7.5, 10 % D_2O.

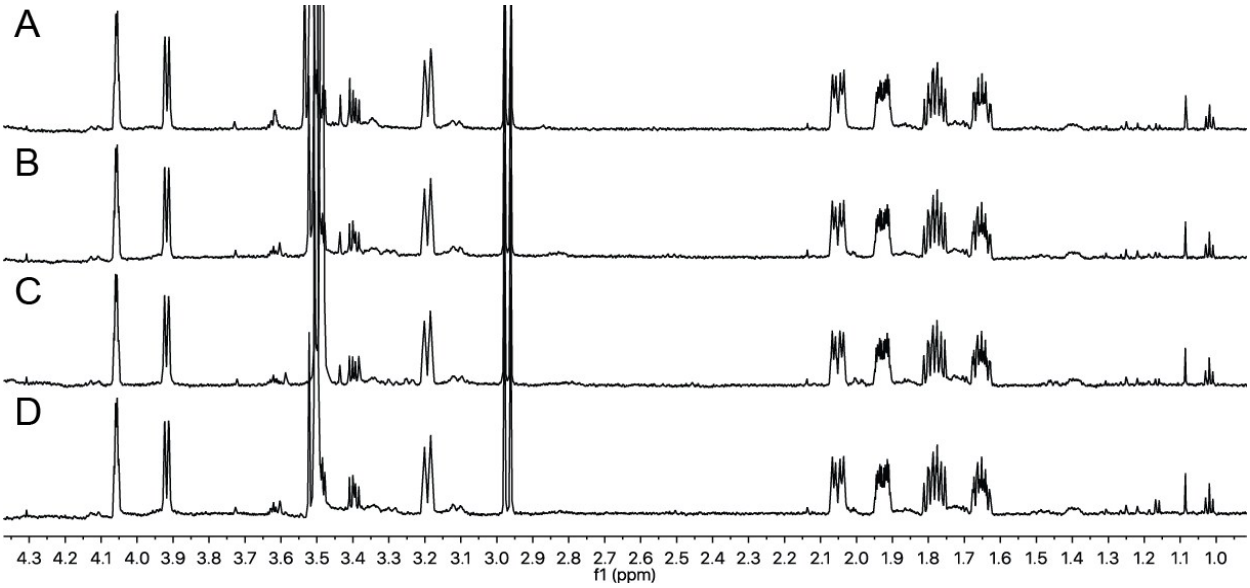

Figure S5. Stability of avibactam to OXA catalysis. ^{1}H-NMR spectra (700 MHz) of 400 μM avibactam incubated at room temperature for 22 h with (A) no enzyme, (B) 10 μM OXA-48, (C) 10 μM OXA-23, and (D) 10 μM OXA-10 in 50 mM Tris-d_{11}, pH 7.5, 10 % D_2O with 10 mM $NaHCO_3$. No detected avibactam hydrolysis was observed within limits of detection with any of the tested OXA β-lactamases (< 5 %).

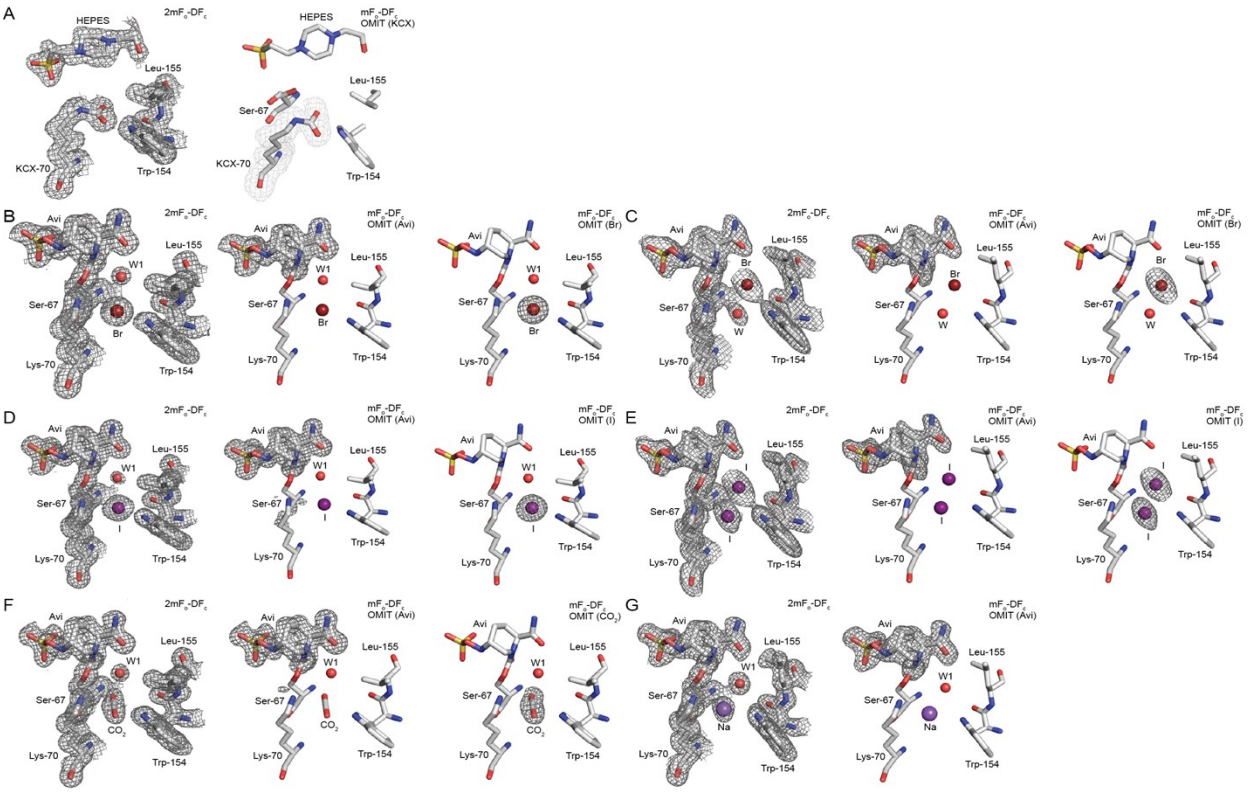

Figure S6. Electron density maps for the active sites from OXA crystal structures. 2mF$_o$-DF$_c$ (contoured to 1.0 σ) and mF$_o$-DF$_c$ OMIT (contoured to 3.0 σ) electron density maps representing views from the OXA-10 crystal structures. (A) Chain A of OXA-10 with bound HEPES (PDB 5MMY), (B, C) chains A and B of OXA-10 avibactam complex with bound bromide ions (PDB 5MNU), (D, E) chains A and B of OXA-10 avibactam complex with bound iodide ions (PDB 5MOZ), and (F, G) chains A and B of OXA-10 avibactam complex with bound CO_2 and sodium, respectively (PDB 5MOX). Avibactam is labelled with Avi, water with W, and the carbamylated lysine (Lys-70) with KCX.

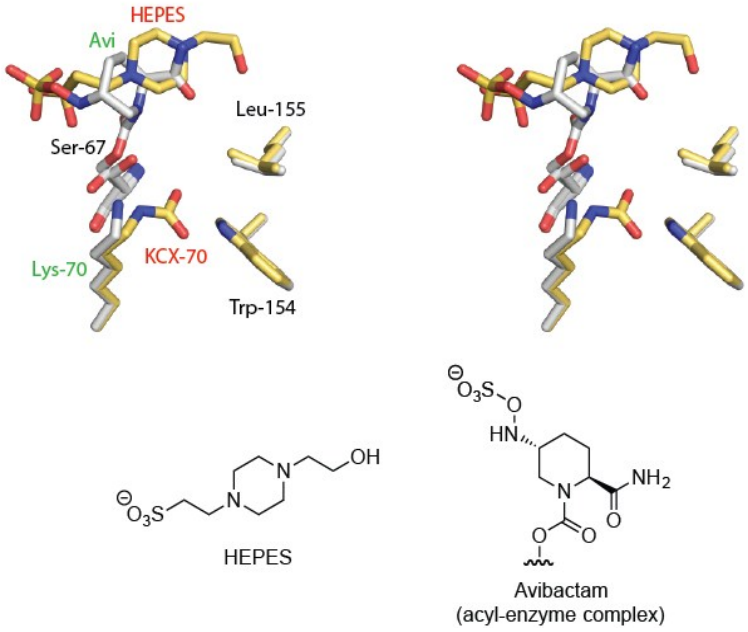

Figure S7. Overlay of HEPES and avibactam binding conformations in OXA-10 structures. Stereo diagram of views of the OXA-10 crystal structure active site showing similar binding modes of HEPES (PDB 5MMY, chain A; yellow carbons) and the avibactam-derived complex (PDB 5MNY, chain A; white carbons). Features specific to the HEPES structure are labelled in red, and those specific to the avibactam complex are labelled in green. Note that Lys-70 is carbamylated in the HEPES complex, but not in the avibactam complex.

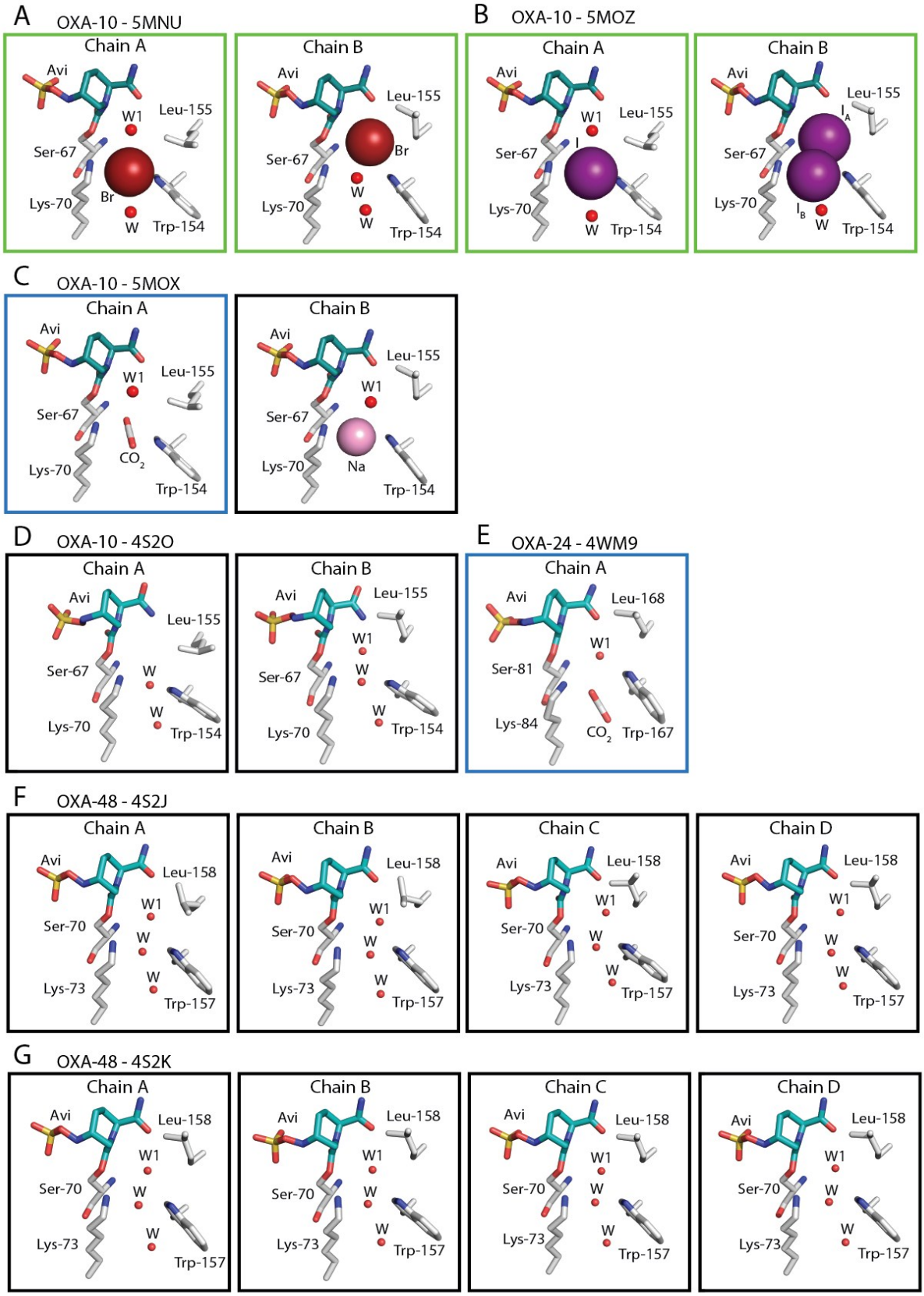
A
OXA-10 - 5MNU
Chain A
Avi
W1
Leu-155
Ser-67
Br
Lys-70
Br
W
Trp-154
Chain B
Avi
Leu-155
Ser-67
Br
W
Lys-70
W
Trp-154
B
OXA-10 - 5MOZ
Chain A
Avi
W1
Leu-155
Ser-67
I
Lys-70
W
Trp-154
Chain B
Avi
Leu-155
I_A
Ser-67
Lys-70
I_B
W
Trp-154
C
OXA-10 - 5MOX
Chain A
Avi
W1
Leu-155
Ser-67
CO_2
Lys-70
Trp-154
Chain B
Avi
Leu-155
W1
Ser-67
Lys-70
Na
Trp-154
D
OXA-10 - 4S2O
Chain A
Avi
Leu-155
Ser-67
W
W
Lys-70
Trp-154
Chain B
Avi
Leu-155
W1
Ser-67
W
W
Lys-70
Trp-154
E
OXA-24 - 4WM9
Chain A
Avi
Leu-168
W1
Ser-81
Lys-84
CO_2
Trp-167
F
OXA-48 - 4S2J
Chain A
Avi
Leu-158
W1
Ser-70
W
Lys-73
W
Trp-157
Chain B
Avi
Leu-158
W1
Ser-70
W
Lys-73
W
Trp-157
Chain C
Avi
Leu-158
W1
Ser-70
W
Lys-73
W
Trp-157
Chain D
Avi
Leu-158
W1
Ser-70
W
Lys-73
W
Trp-157
G
OXA-48 - 4S2K
Chain A
Avi
Leu-158
W1
Ser-70
W
Lys-73
W
Trp-157
Chain B
Avi
Leu-158
W1
Ser-70
W
Lys-73
W
Trp-157
Chain C
Avi
Leu-158
W1
Ser-70
W
Lys-73
W
Trp-157
Chain D
Avi
Leu-158
W1
Ser-70
W
Lys-73
W
Trp-157

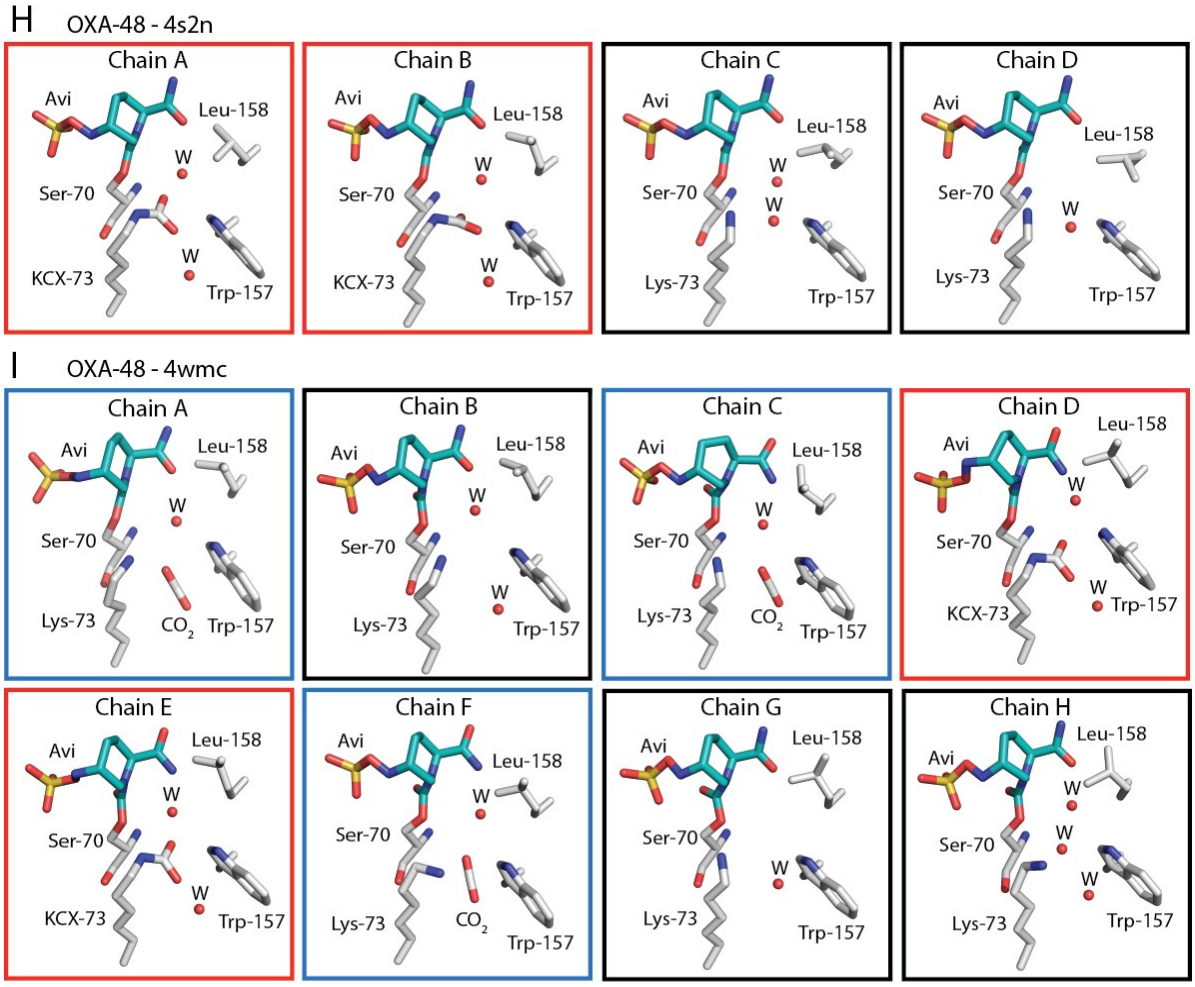

Figure S8. Conformations of avibactam in OXA crystal structures. Views from crystal structures showing the observed conformations of avibactam in complex with OXA-10, compared with those in reported OXA-10, OXA-23, and OXA-48 avibactam complex structures.[15, 16] Views from our structures of the OXA-10:avibactam complex with bound (A) bromide ions, (B) iodide ions, and (C) sodium ions and carbon dioxide. Note the iodide ions occupy one of two shown positions – refined occupancies of 70 % and 30 % for I_A and I_B, respectively. Note that we cannot rule out partial low level occupancies by other species in the assigned halide/sodium ion binding sites. Active site views from reported crystal structures[15, 16] of (D) OXA-10, (E) OXA-24, and (F, G, H, I) OXA-48 avibactam complexes. Structures with

carbamylated lysine residues have a red border, structures with bound carbon dioxide have a blue border, and structures with bound halide ions have a green border. Note that the orientation of N6 of avibactam (numbering in Figure 1C) is suitable for recyclisation in some structures (e.g., A, B, C, F, G, H, and some chains of I), while this nitrogen is rotated away from the carbamoylated serine residue in others (e.g., D, E, and some chains of I).

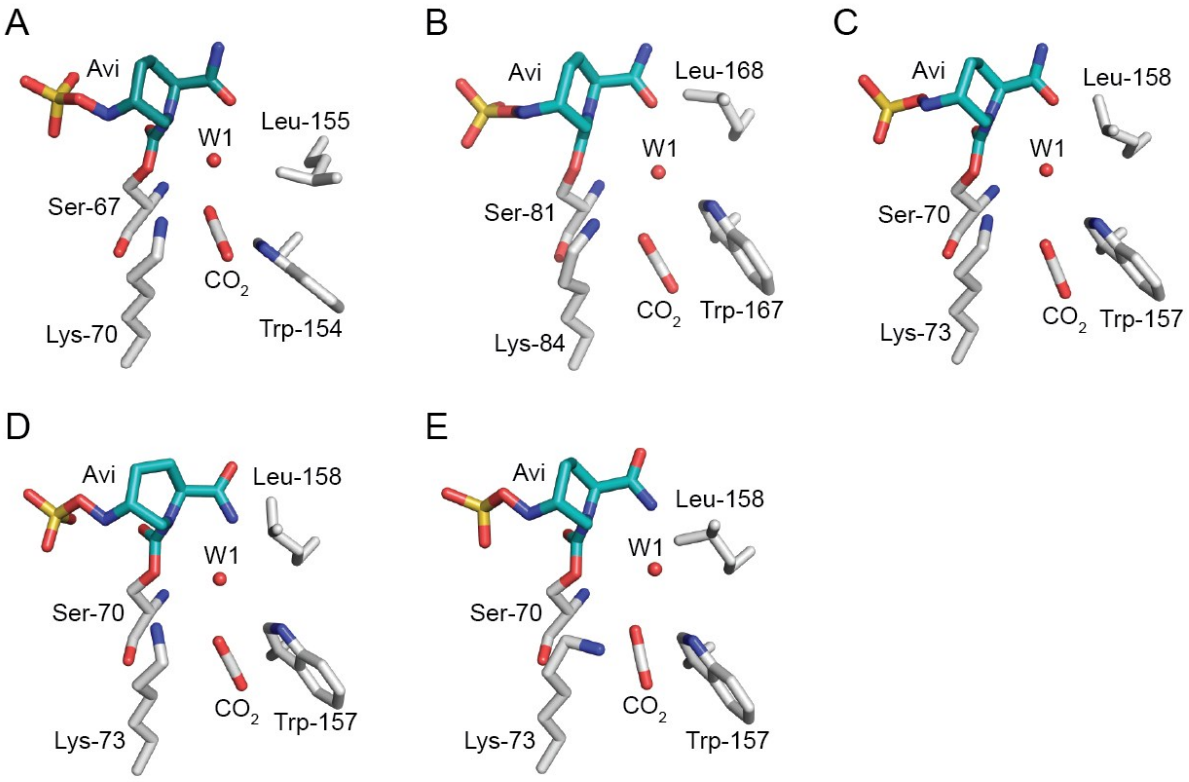

Figure S9. OXA avibactam complexes with bound carbon dioxide. Active site views from crystal structures of (A) OXA-10 (PDB 5MOX, chain A), (B) OXA-24 (PDB 4WM9, chain A), (C, D, E) OXA-48 (PDB 4WMC, chains A, C, and F, respectively) avibactam complexes.[16]

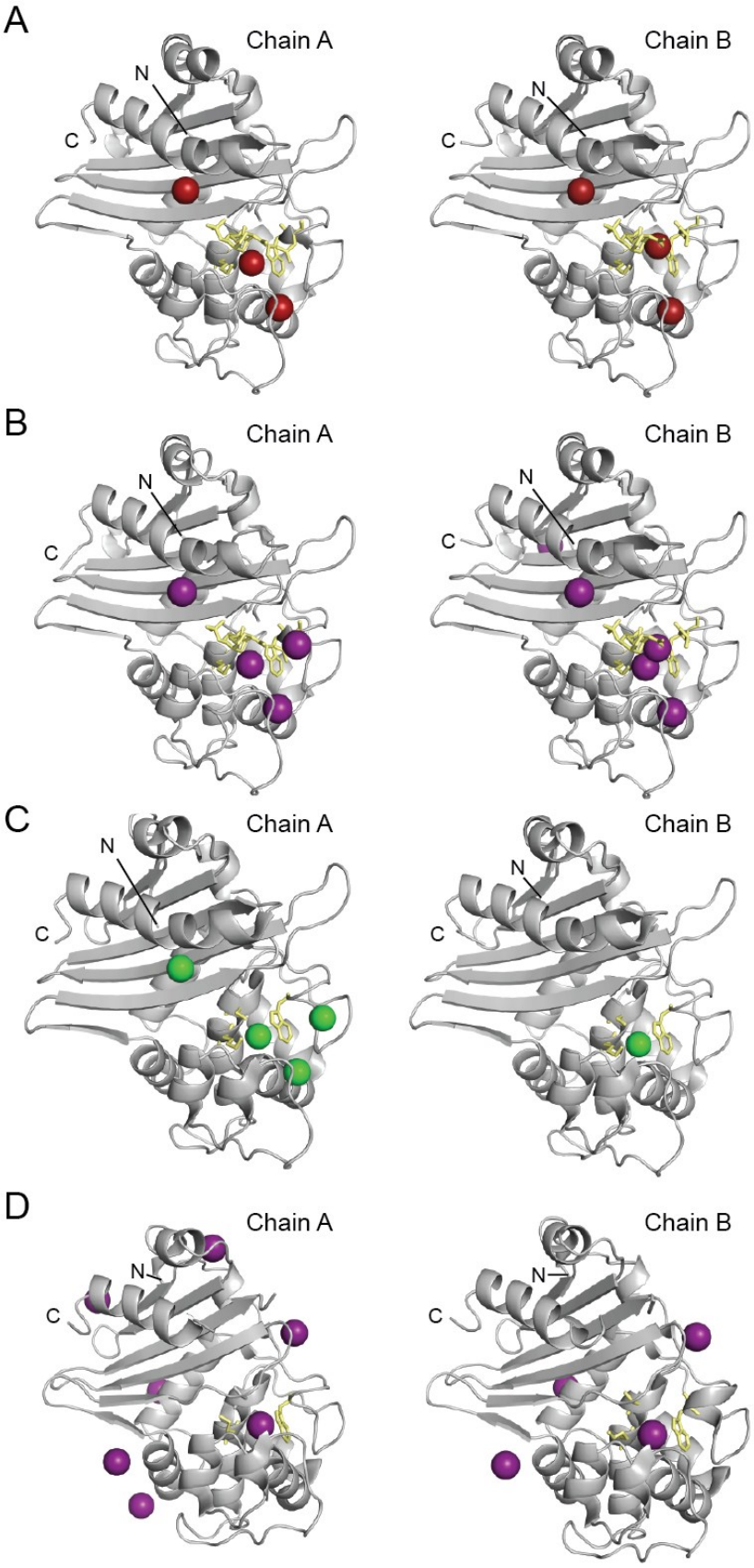
A
Chain A
N
C
Chain B
N
C
B
Chain A
N
C
Chain B
N
C
C
Chain A
N
C
Chain B
N
C
D
Chain A
N
C
Chain B
N
C

Figure S10. Multiple binding sites of halide ions to OXA-enzymes. Overall views from crystal structures of the OXA-10:avibactam complexes described herein with bound (A) bromide ions (PDB 5MNU), and (B) iodide ions (PDB 5MOZ). Overall views of the reported crystal structures of (C) V117T OXA-10 with bound chloride ions (PDB 2WGV),[17] and (D) OXA-163 with bound iodide ions (PDB 4S2M).[18] Selected active site residues (Ser-67, Lys-70, Trp-154; OXA-10 numbering) and avibactam are in yellow. Note the halide ions can bind at more than one position in the active site and at sites away from the active site, and that we cannot rule out the presence of ions at relatively low occupancy levels at the assigned ion binding sites.

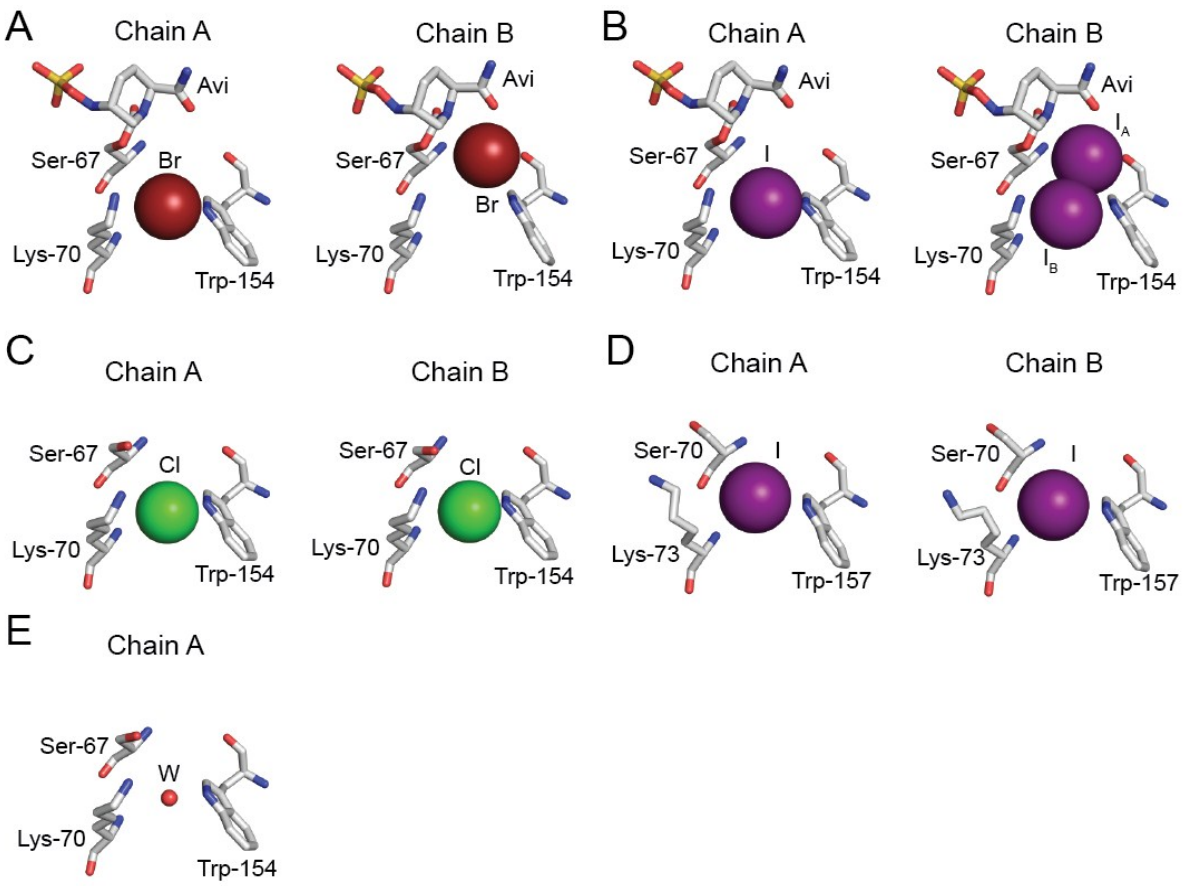

Figure S11. OXA active site halide binding sites. Active site views from the OXA-10 crystal structures described herein showing the active site halide binding sites compared with those previously reported.[17, 18] Active site views from the structures of the OXA-10:avibactam complex with bound (A) bromide ions (PDB 5MNU), and (B) iodide ions (PDB 5MOZ; refined occupancies of 70 % and 30 % for I_A and I_B, respectively). Active site views for reported structures of OXA:halide ion complexes showing (C) V117T OXA-10 with a bound chloride ion (PDB 2WGV),[17] (D) OXA-163 with a bound iodide ion (PDB 4S2M),[18] and (E) OXA-10 with a bound water molecule (W; PDB 1FOF).[19] Paetzel *et al.* observed that the Lys-70 associated water molecule (panel E) may be replaced with a chloride ion.[19]

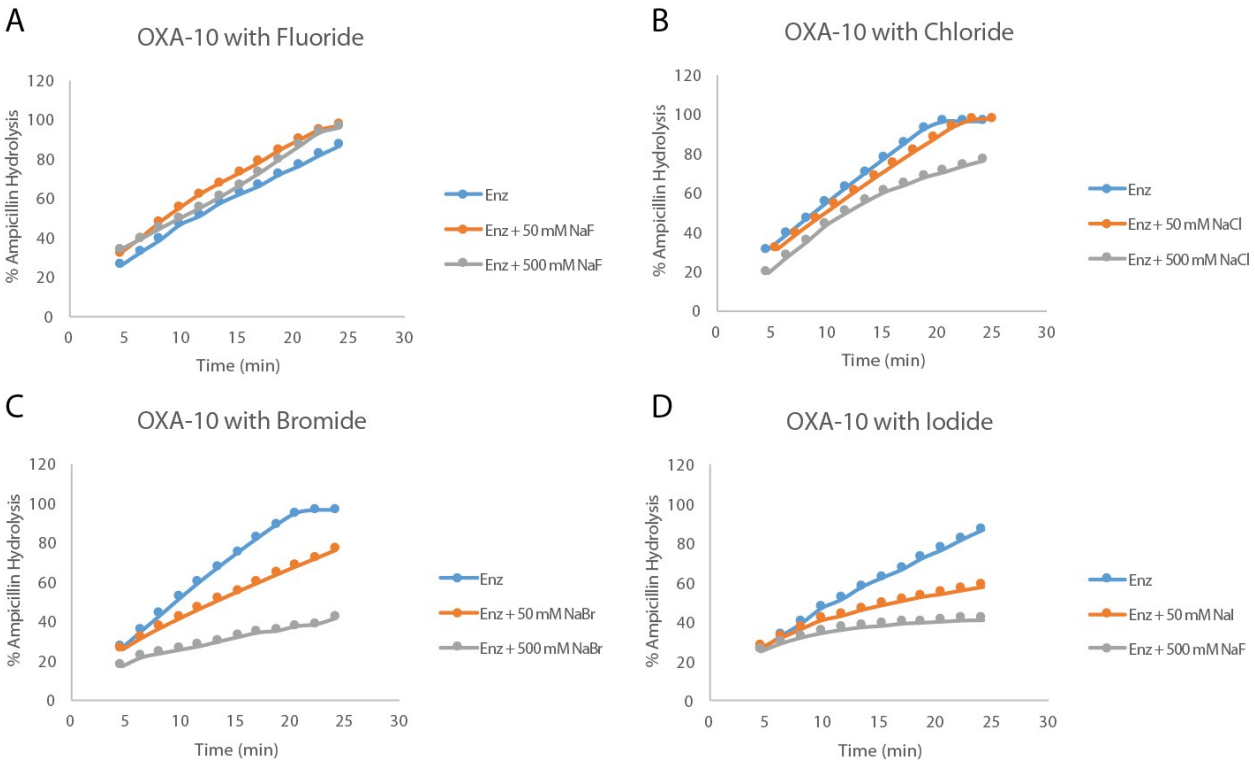

Figure S12. Effects of halide ions on OXA-10 catalysis. The impact of (A) fluoride, (B) chloride, (C) bromide, and (D) iodide ions on OXA-10 catalysed hydrolysis of ampicillin as observed by ^{1}H-NMR (700 MHz). Reaction mixtures consisted of 75 nM enzyme, 50 mM or 500 mM of the appropriate sodium halide and 10 mM ampicillin in 50 mM Tris-d_{11}, pH 7.5, 10 % D_2O.

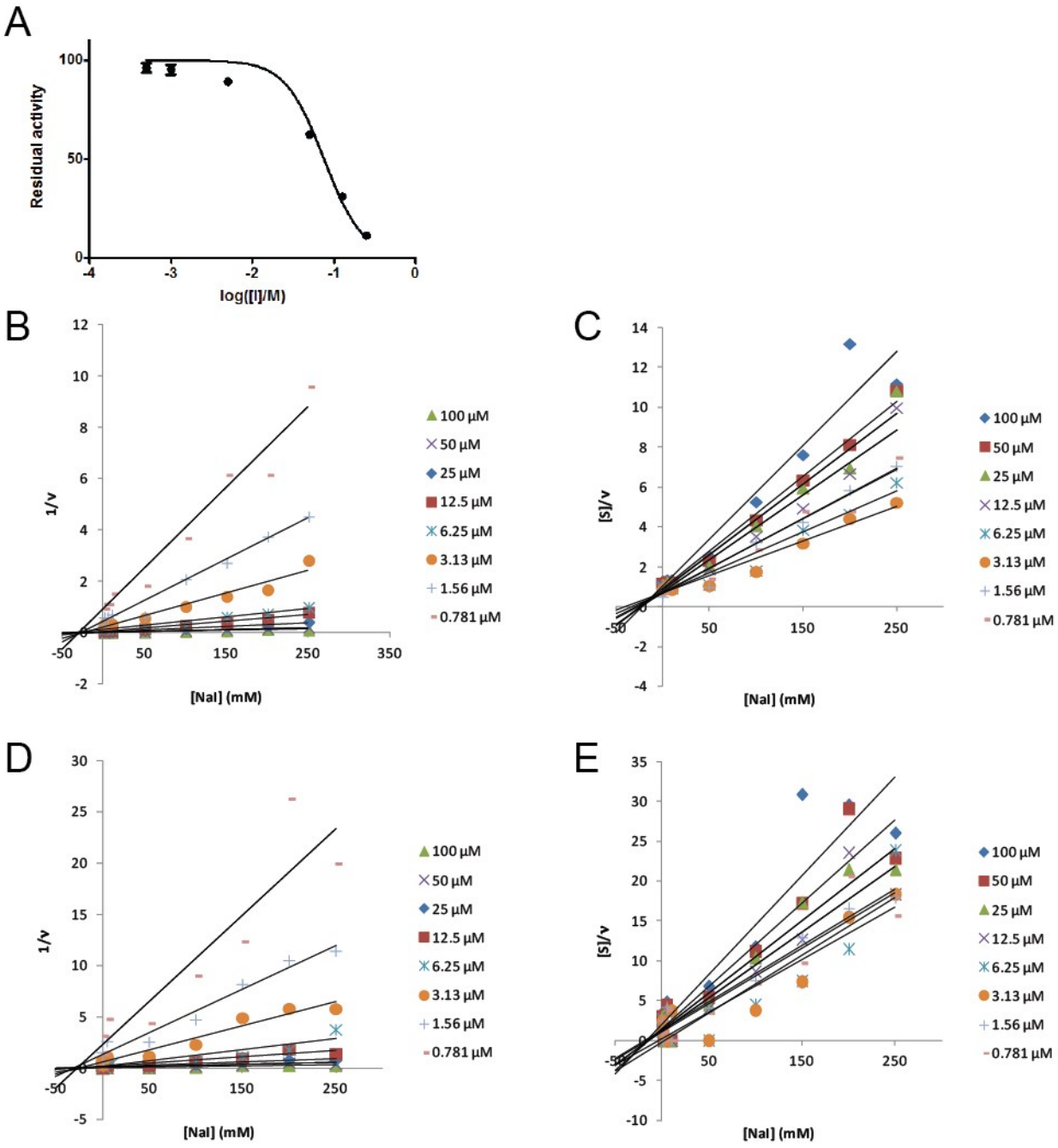

Figure S13. Mode of OXA-23 inhibition by iodide ions. Kinetic characterisation of the inhibition of OXA-23 by iodide ions, showing (A) IC_{50} determination, (B) Dixon plot, and (C) Cornish-Bowden plot. Replicates of the (D) Dixon plot and the (E) Cornish-Bowden plot are also shown. GraphPad Prism 5 (GraphPad Software) was used for IC_{50} determination.

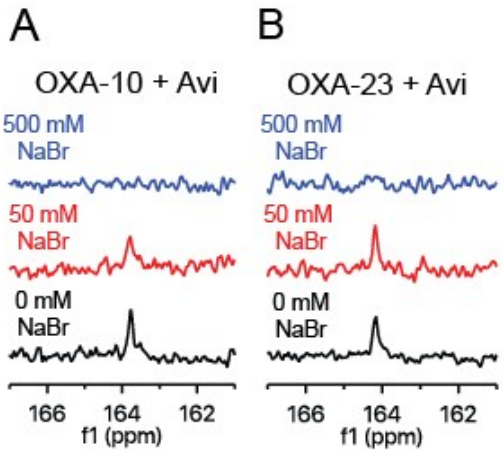

Figure S14. Decarbamylation of OXA-10 by sodium bromide. ^{13}C-NMR spectra (600 MHz) showing the impact of 0, 50, and 500 mM sodium bromide on 800 μM ^{13}C-labeled (A) OXA-10 and (B) OXA-23, in the presence of 15 mM avibactam, 50 mM sodium phosphate, pH 7.5, 10 mM $NaH^{13}CO_3$, and 10 % D_2O.

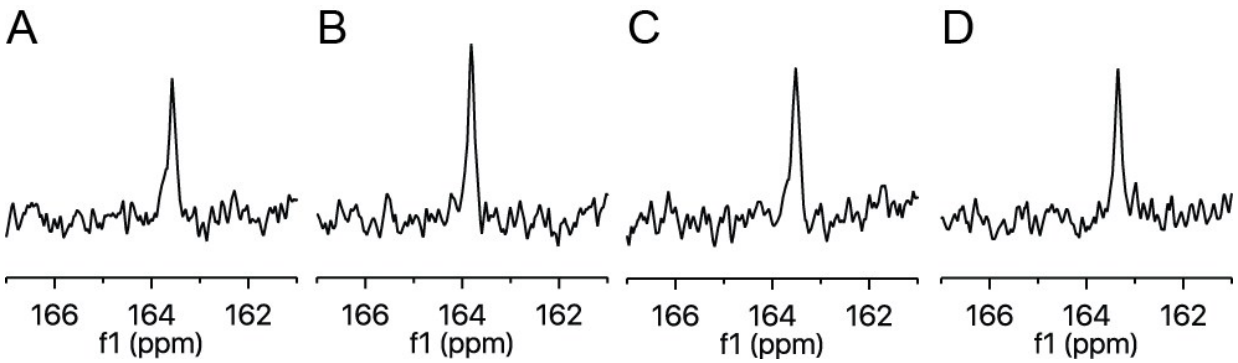

Figure S15. Impact of alkali metals on OXA carbamylation. (A) ^{13}C-NMR spectrum (600 MHz) for ^{13}C-labelled OXA-23 (800 μM; in 50 mM sodium phosphate, pH 7.5, 10 mM $NaH^{13}CO_3$, 10 % D_2O). ^{13}C-NMR spectra (600 MHz) for OXA-23 (800 μM; in 25 mM HEPES, pH 7.5, 100 mM NaCl, 10 % D_2O) with (B) no added salts, (C) 200 mM sodium phosphate, pH 7.4, and (D) 200 mM potassium phosphate, pH 7.4.

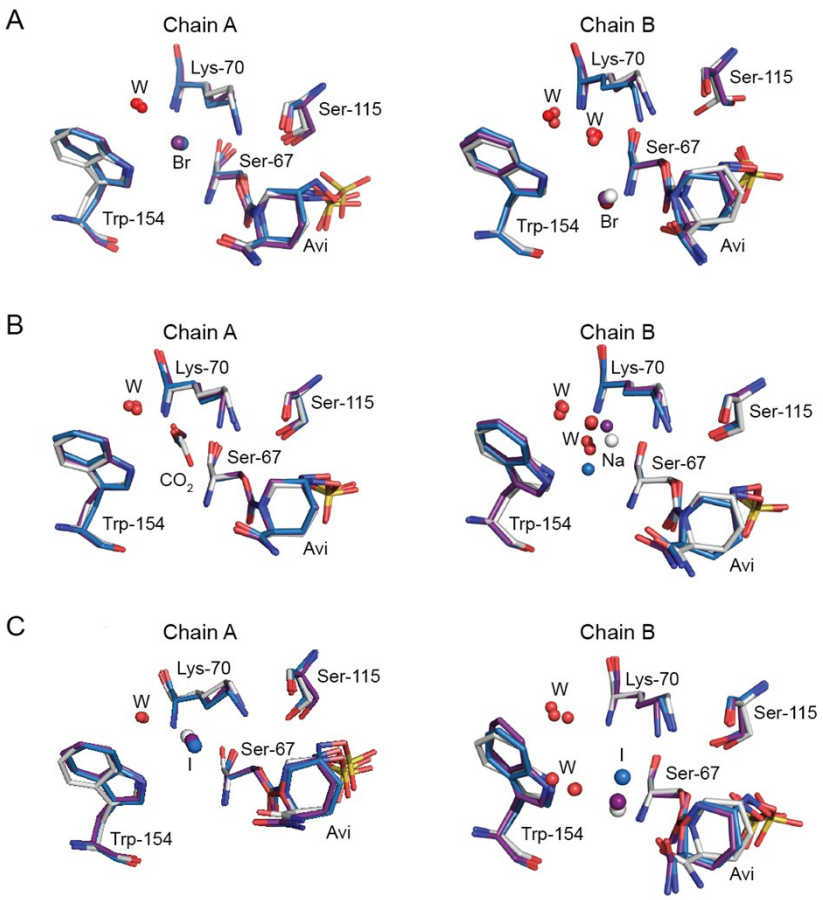

Figure S16. Results from QM/MM geometry optimization calculations on the OXA-10 active site. Overlays of active site conformations for systems with neutral Nε Lys-70 (purple) and protonated Nε (blue) Lys-70 compared to the refined crystal structure (white). The QM region comprised Ser-67 reacted with avibactam, Lys-70, Ser-115, Trp-154 and up to three water molecules. Calculations with a neutral Lys-70 Nε amino group resulted in optimized ion-Lys-70 distances consistently closer to those observed in crystal structures than with a protonated Lys-70 (Table S5). Water molecules are indicated in red.

Table S1. Kinetic characterization of OXA substrates using nitrocefin and FC5 as substrates.[20]

	kcat (s^{-1})	Vmax ($\mu M\ s^{-1}$)	Km (μM)	kcat/Km ($s^{-1}\ M^{-1}$)
OXA-23 (no $NaHCO_3$)				
Nitrocefin	759	1.518 ± 0.118	15.21 ± 4.89	4.99×10^7
FC5	78	0.975 ± 0.062	25.04 ± 2.63	3.12×10^6
OXA-23 (50 mM $NaHCO_3$)				
Nitrocefin	2793	5.586 ± 0.318	49.99 ± 9.38	5.59×10^7
FC5	79.39	0.992 ± 0.107	22.3 ± 3.41	3.56×10^6
OXA-48 (no $NaHCO_3$)				
Nitrocefin	1919	3.838 ± 0.275	27.06 ± 7.35	7.09×10^7
FC5	76.58	0.957 ± 0.067	31.5 ± 3.42	2.43×10^6
OXA-48 (50 mM $NaHCO_3$)				
Nitrocefin	4806	9.612 ± 0.412	61.64 ± 8.27	7.80×10^7
FC5	108.6	1.358 ± 0.199	48.13 ± 8.52	2.26×10^6

Table S2. Data collection and refinement statistics

Structure	**OXA-10−EPE**	**OXA-10−AVI_I**	**OXA-10−AVI_BR**	**OXA-10−AVI_CO**
PDB ID	5MMY	5MOZ	5MNU	5MOX
Radiation Source	Diamond I04	Diamond I04	Diamond I04	Diamond I04
Resolution Range (Å)	51.09 - 1.88 (1.94 - 1.88)‡	53.77 - 1.34 (1.38 - 1.34)	63.61 - 1.56 (1.61 - 1.56)‡	76.76 - 1.41 (1.46 - 1.41)
Space group	$P\,2_1\,2_1\,2_1$	$P\,2_1\,2_1\,2_1$	$P\,2_1\,2_1\,2_1$	$P\,2_1\,2_1\,2_1$
Unit cell dimensions				
a,b,c (Å)	48.77 102.12 127.4	48.84 101.65 126.72	48.77 101.42 127.21	48.75 96.63 126.36
α,β,γ (°)	90 90 90	90 90 90	90 90 90	90 90 90
No. of molecules/ASU	2	2	2	2
No. of unique reflections	52491 (5120)‡	141885 (13962)	90636 (8954)‡	115719 (11449)‡
Completeness (%)	100 (99.7)‡	99.9 (99.2)‡	100 (100)‡	100 (100)‡
Redundancy	12.9(11.5)‡	12.8(12.1)‡	13.0(13.0)‡	12.9(12.6)‡
R_{merge}	0.172(2.092)‡	0.103(2.828)‡	0.162(2.789)‡	0.184(3.083)‡
Mean I/σ(I)	11.8(3.2)‡	11.2(1.1)‡	9(1.3)‡	9.5(1.2)‡
$CC_{1/2}$	0.99(0.76)	0.99(0.46)	0.99(0.53)	0.99(0.51)
Wilson B value (Å^2)	18.08	15.21	17.86	12.22
Refinement				
R_{factor}	0.1778 (0.2963)‡	0.1663 (0.3733)‡	0.1850 (0.3691)‡	0.1573 (0.3254)‡
R_{free}	0.1979 (0.2604)‡	0.1839 (0.3819)‡	0.2081 (0.3593)‡	0.1897 (0.3599)‡
R.m.s.d.				
Bond length (Å)	0.006	0.012	0.004	0.008
Bond angle (°)	0.766	1.191	0.748	1.156
Total no. of atoms	4205	4551	4504	4621
Protein	3847	3917	3889	3921
Ligand/ion	56	98	101	69
Water	302	536	514	631
Ramachandran allowed (%)	97	97	98	98
Ramachandran outliers (%)	3.2	2.6	2	2.2
Rotamer outliers (%)	0	0	0	0.2
$<B_{factor}>$ (Å^2)				
Protein	31.70	26.37	30.19	16.87
Ligand/ion	41.19	32.13	38.80	24.92
Water	36.03	35.90	36.78	32.10

R_{merge} is the unweighted R-value on I between merged reflections.
$R_{factor} = \Sigma_{hkl} \mid |F_{obs}(hkl)| - |F_{calc}(hkl)| \mid / \Sigma_{hkl} |F_{obs}(hkl)|$ for the working set of reflections.
‡ outermost shell.

Table S3. Details of the systems studied included in the analyses on the protonation state of Lys-70, the number of atoms in the QM region, the total number of atoms in the system, and the active site atom or molecule unique to each system.

Chain	Lys-70 protonation state	QM atoms	System Size	Particle
A – Br^-	Neutral	74	48194	Br^-
B – Br^-		77	48080	Br^-
A – CO_2		80	48192	CO_2
B – CO_2		80	48252	Na^+
A – I^-		74	48135	I^-
B – I^-		74	48130	I^-
A – Br^-	Protonated	75	48195	Br^-
B – Br^-		78	48081	Br^-
A – CO_2		81	48193	CO_2
B – Na^+		81	48253	Na^+
A – I^-		75	48136	I^-
B – I^-		75	48131	I^-

Table S4. Description of QM region including total charge for each system considered with protonated Lys-70 ($-NH_3^+$; top two tables) and neutral Lys-70 ($-NH_2$; bottom two tables).

Protonated:

Chain A	**Br**	**Charge**	**CO_2**	**Charge**	**I**	**Charge**
QM Region	Ser-67	-1	Ser-67	-1	Ser-67	-1
	Lys-70	+1	Lys-70	+1	Lys-70	+1
	Ser-115	0	Ser-115	0	Ser-115	0
	Trp-154	0	Trp-154	0	Trp-154	0
	Br^-	-1	CO_2	0	I^-	-1
	Wat32	0	Wat31	0	Wat27	0
Total charge		-1		0		-1

Chain B	**Br**	**Charge**	**Na**	**Charge**	**I**	**Charge**
QM Region	Ser-67	-1	Ser-67	-1	Ser-67	-1
	Lys-70	+1	Lys-70	+1	Lys-70	1
	Ser-115	0	Ser-115	0	Ser-115	0
	Trp-154	0	Trp-154	0	Trp-154	0
	Br^-	-1	Na^+	+1	I^-	-1
	Wat202	0	Wat618	0	Wat348	0
	Wat492	0	Wat176	0		
			Wat56	0		
Total charge		-1		1		-1

Neutral:

Chain A	**Br^-**	**Charge**	**CO_2**	**Charge**	**I^-**	**Charge**
QM Region	Ser-67	-1	Ser-67	-1	Ser-67	-1
	Lys-70	0	Lys-70	0	Lys-70	0
	Ser-115	0	Ser-115	0	Ser-115	0
	Trp-154	0	Trp-154	0	Trp-154	0
	Br^-	-1	CO_2	0	I^-	-1
	Wat32	0	Wat31	0	Wat27	0
Total charge		-2		-1		-2

Chain B	**Br^-**	**Charge**	**Na^+**	**Charge**	**I^-**	**Charge**
QM Region	Ser-67	-1	Ser-67	-1	Ser-67	-1
	Lys-70	0	Lys-70	0	Lys-70	0
	Ser-115	0	Ser-115	0	Ser-115	0
	Trp-154	0	Trp-154	0	Trp-154	0
	Br^-	-1	Na^+	+1	I^-	-1
	Wat202	0	Wat618	0	Wat348	0
	Wat492	0	Wat176	0	Wat302	0
			Wat56	0		
Total charge		-2		0		-2

Table S5. Comparison of the Lys-70-ion distances as observed in the crystalline state (PDB 5MNU, 5MOX, 5MOZ) and from the QM/MM calculations. The distances were measured from the Lys-70 Nε atom (top table) and from the Lys-70 Cα atom (bottom table).

Lys-70 Nε distances:

Chain	Lys-70 protonation state	Particle	Crystallographic Lys-70-ion distance (Å)	QM/MM Optimized Lys-70-ion distance (Å)	Deviation (Å)
A – Br^-	Neutral	Br^-	3.2	3.4	0.2
B – Br^-		Br^-	4.9	4.9	0.0
A – CO_2		CO_2	2.9	2.8	-0.1
B – Na^+		Na^+	2.9	2.4	-0.5
A – I^-		I^-	3.4	3.5	0.1
B – I^-		I^-	4.7	3.8	-0.9
A – Br^-	Protonated	Br^-	3.2	3.1	-0.1
B – Br^-		Br^-	4.9	4.5	-0.4
A – CO_2		CO_2	2.9	3.3	0.4
B – Na^+		Na^+	2.9	4.4	1.5
A – I^-		I^-	3.4	3.3	-0.1
B – I^-		I^-	4.7	3.3	-0.1

Lys-70 Cα distances:

Chain	Lys-70 protonation state	Particle	Crystallographic Lys-70-ion distance (Å)	QM/MM Optimized Lys-70-ion distance (Å)	Deviation (Å)
A – Br^-	Neutral	Br^-	5.4	5.9	0.4
B – Br^-		Br^-	7.6	7.6	0.0
A – CO_2		CO_2	5.4	5.3	-0.1
B – Na^+		Na^+	5.2	4.9	-0.3
A – I^-		I^-	5.6	6.4	0.8
B – I^-		I^-	7.6	7.6	0.0
A – Br^-	Protonated	Br^-	5.4	5.7	0.3
B – Br^-		Br^-	7.6	7.6	0.0
A – CO_2		CO_2	5.4	5.3	-0.1
B – Na^+		Na^+	5.2	6.4	1.2
A – I^-		I^-	5.6	6.4	0.8
B – I^-		I^-	7.5	6.2	0.7

References

(1) Hutter, J.; Iannuzzi, M.; Schiffmann, F., and VandeVondele, J. (2014) CP2K: atomistic simulations of condensed matter systems *WIREs Comput. Mol. Sci. 4*, 15-25.

(2) Humphrey, W.; Dalke, A., and Schulten, K. (1996) VMD: visual molecular dynamics. *J. Mol. Graph. 14*, 33-8, 27.

(3) VandeVondele, J.; Krack, M.; Mohamed, F.; Parrinello, M.; Chassaing, T., and Hutter, J. (2005) Quickstep: Fast and accurate density functional calculations using a mixed Gaussian and plane waves approach *Comp. Phys. Comm. 167*, 103-128.

(4) Krack, M., and Parrinello, M. (2004) Quickstep: make the atoms dance *High Perform. Comput. Chem. 25*, 29.

(5) Laio, A.; VandeVondele, J., and Rothlisberger, U. (2002) A Hamiltonian electrostatic coupling scheme for hybrid Car–Parrinello molecular dynamics simulations. *J. Chem. Phys. 116*, 6941-6947.

(6) Laino, T.; Mohamed, F.; Laio, A., and Parrinello, M. (2005) An efficient real space multigrid QM/MM electrostatic coupling. *J. Chem. Theory Comput. 1*, 1176-1184.

(7) Lee, C.; Yang, W., and Parr, R. G. (1988) Development of the Colle-Salvetti correlation-energy formula into a functional of the electron density. *Phys. Rev. B Condens. Matter. 37*, 785-789.

(8) Becke, A. D. (1988) Density-functional exchange-energy approximation with correct asymptotic behavior. *Phys. Rev. A Gen. Phys. 38*, 3098-3100.

(9) Hartwigsen, C.; Gœdecker, S., and Hutter, J. (1998) Relativistic separable dual-space Gaussian pseudopotentials from H to Rn *Phys. Rev. B*

(10) Goedecker; Teter, and Hutter. (1996) Separable dual-space Gaussian pseudopotentials. *Phys. Rev. B Condens. Matter 54*, 1703-1710.

(11) Brooks, B. R.; Brooks, C. L.; Mackerell, A. D.; Nilsson, L.; Petrella, R. J.; Roux, B.; Won, Y.; Archontis, G.; Bartels, C.; Boresch, S.; Caflisch, A.; Caves, L.; Cui, Q.; Dinner, A. R.; Feig, M.; Fischer, S.; Gao, J.; Hodoscek, M.; Im, W.; Kuczera, K.; Lazaridis, T.; Ma, J.; Ovchinnikov, V.; Paci, E.; Pastor, R. W.; Post, C. B.; Pu, J. Z.; Schaefer, M.; Tidor, B.; Venable, R. M.; Woodcock, H. L.; Wu, X.; Yang, W.; York, D. M., and Karplus, M. (2009) CHARMM: the biomolecular simulation program. *J. Comput. Chem. 30*, 1545-1614.

(12) Maseras, F., and Morokuma, K. (1995) IMOMM: A new integrated ab initio+ molecular mechanics geometry optimization scheme of equilibrium structures and transition states *J. Comput. Chem. 16*, 1170-1179.

(13) Ehmann, D. E.; Jahic, H.; Ross, P. L.; Gu, R. F.; Hu, J.; Durand-Réville, T. F.; Lahiri, S.; Thresher, J.; Livchak, S.; Gao, N.; Palmer, T.; Walkup, G. K., and Fisher, S. L. (2013) Kinetics of avibactam inhibition against class A, C, and D β-lactamases. *J. Biol. Chem. 288*, 27960-27971.

(14) Abboud, M. I.; Damblon, C.; Brem, J.; Smargiasso, N.; Mercuri, P.; Gilbert, B.; Rydzik, A. M.; Claridge, T. D.; Schofield, C. J., and Frère, J. M. (2016) Interaction of Avibactam with Class B Metallo-β-Lactamases. *Antimicrob. Agents Chemother. 60*, 5655-5662.

(15) King, D. T.; King, A. M.; Lal, S. M.; Wright, G. D., and Strynadka, N. C. J. (2015) Molecular mechanism of avibactam-mediated β-lactamase inhibition *ACS Infect. Dis. 1*, 175-184.

(16) Lahiri, S. D.; Mangani, S.; Jahić, H.; Benvenuti, M.; Durand-Reville, T. F.; De Luca, F.; Ehmann, D. E.; Rossolini, G. M.; Alm, R. A., and Docquier, J. D. (2015) Molecular basis of selective inhibition and slow reversibility of avibactam against class D carbapenemases: a structure-guided study of OXA-24 and OXA-48. *ACS Chem. Biol. 10*, 591-600.
(17) Vercheval, L.; Bauvois, C.; di Paolo, A.; Borel, F.; Ferrer, J. L.; Sauvage, E.; Matagne, A.; Frère, J. M.; Charlier, P.; Galleni, M., and Kerff, F. (2010) Three factors that modulate the activity of class D β-lactamases and interfere with the post-translational carboxylation of Lys70. *Biochem. J. 432*, 495-504.
(18) Stojanoski, V.; Chow, D. C.; Fryszczyn, B.; Hu, L.; Nordmann, P.; Poirel, L.; Sankaran, B.; Prasad, B. V., and Palzkill, T. (2015) Structural basis for different substrate profiles of two closely related class D β-lactamases and their inhibition by halogens. *Biochemistry 54*, 3370-3380.
(19) Paetzel, M.; Danel, F.; de Castro, L.; Mosimann, S. C.; Page, M. G., and Strynadka, N. C. (2000) Crystal structure of the class D β-lactamase OXA-10. *Nat. Struct. Biol. 7*, 918-925.
(20) van Berkel, S. S.; Brem, J.; Rydzik, A. M.; Salimraj, R.; Cain, R.; Verma, A.; Owens, R. J.; Fishwick, C. W.; Spencer, J., and Schofield, C. J. (2013) Assay platform for clinically relevant metallo-β-lactamases. *J. Med. Chem. 56*, 6945-6953.